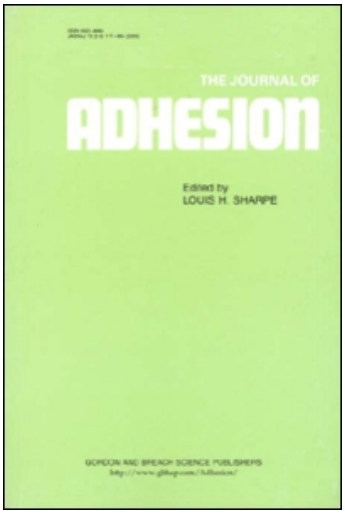

The Journal of Adhesion

Publication details, including instructions for authors and subscription information:
http://www.informaworld.com/smpp/title~content=t713453635

A Comparison Between Measurements and Finite Element Predictions of Crack Opening Displacements Near the Front of an Interface Crack

K. M. Liechti[a]; D. Ginsburg[a]; E. C. Hanson[a]
[a] Department of Aerospace Engineering and Engineering Mechanics, The University of Texas at Austin, Austin, Texas, U.S.A.

To cite this Article Liechti, K. M. , Ginsburg, D. and Hanson, E. C.(1987) 'A Comparison Between Measurements and Finite Element Predictions of Crack Opening Displacements Near the Front of an Interface Crack', The Journal of Adhesion, 23: 2, 123 — 146
To link to this Article: DOI: 10.1080/00218468708075401
URL: http://dx.doi.org/10.1080/00218468708075401

J. Adhesion, 1987, Vol. 23, pp. 123–146
Photocopying permitted by license only

Printed in the United Kingdom

A Comparison Between Measurements and Finite Element Predictions of Crack Opening Displacements Near the Front of an Interface Crack†

K. M. LIECHTI,‡ D. GINSBURG and E. C. HANSON

Department of Aerospace Engineering and Engineering Mechanics, The University of Texas at Austin, Austin, Texas 78712, U.S.A.

(*Received November 7, 1986*)

Crack opening displacements close to the front of an interface crack between glass and epoxy determined from measurements and finite-element solutions are compared. The measurements were made using optical interferometry, and the finite-element solutions were based on a linear material response and the displacements that were applied during crack initiation experiments using a blister test configuration. Various load levels, up to initiation, are considered, and the effect of fracture mode-mix examined by considering different initial crack diameters. The comparisons indicate that a relative increase in the mode II component gave rise to a significant increase in inelastic behavior near the crack front.

KEY WORDS Fracture mechanics; mixed-mode debonding; interface crack initiation; crack opening interferometry, finite-element analysis.

1 INTRODUCTION

Measurements of adhesive fracture energies or critical-strain energy release rates associated with mixed-mode adhesive crack growth

† Presented at the Tenth Annual Meeting of The Adhesion Society, Inc., Williamsburg, Virginia, U.S.A., February 22–27, 1987.

‡ To whom correspondence regarding this paper should be addressed.

have indicated[1,2] that these quantities increase with relative increases in the mode II component. However, if the adhesive fracture energy is thought of as an intrinsic material property that reflects the strength of bonds, then it should be a constant, independent of the fracture mode mixture. The reasons cited for the noted increases include the possibilities of non coplanar crack growth for more brittle materials[1,3] and dissipative effects arising from inelastic material behavior near the crack front.[2] Thus, if the growth of macroscopically coplanar cracks under mixed-mode conditions is to be predicted in a rational manner, such localized phenomena must be accounted for. In view of the increasing use of tougher adhesives, the purpose of the present work is to examine the effect of inelastic material behavior on crack opening displacements close to the crack front through a comparison of direct measurements and linear elastic stress analyses.

Although near-tip singular behavior can be examined using the methods of photoelasticity[4] and caustics,[5] they both involve assumptions as to the constitutive behavior of the materials in the highly stressed crack front region. On the other hand, measurements of displacements are direct, requiring no such assumptions. Since the near-tip region is of interest, the displacements to be measured are small and therefore require the resolution of electron microscopic[6] or optical interferometric techniques.[7–10] Of the latter, crack opening interferometry[9,10] was chosen for the present study because the crack front geometry can be examined. The price for this piece of information is that only the component of crack opening displacements normal to the plane of the crack can be measured. However, this was not felt to be unduly restrictive for the objectives of the present study.

Linear elastic, small deflection analyses of bimaterial bodies containing interface cracks have been conducted over the years for various simple geometries and loadings. The main contributions are summarized in the paper by Piva and Viola.[11] As is well known and discussed by now, all predict a complex singularity in crack front stresses which gives rise to rapid oscillations in the stresses and interpenetration of crack faces as the crack front is approached. If finite deformations are allowed,[12] the complex nature of the singularity has been found to disappear, indicating that the anomalous behavior is due to the linearization of the problem. More

general geometries and loadings have been analyzed by numerical techniques such as boundary collocation[13] and finite-element analysis with hybrid elements[14] which retain the complex singularities. Fracture parameters for interface cracks have also been determined from finite-element analyses that do not make use of special interface crack elements.[15–17] Such procedures can be justified by the small size of the region of interpenetration and the conclusions of Ref. 12. Furthermore, contour integral methods,[15,17] which are relatively insensitive to the exact nature of the stress field at the crack front, are often used to extract stress intensity factors. The finite-element code VISTA[18] was used for the linear elastic analyses in this study.

The details of the specimen geometry, loading and measurement and finite-element procedures are next described in section 2. Measurements of and finite-element solutions for crack opening displacements up to crack initiation and under a range of mixed-mode conditions are then compared in section 3. Conclusions are given in section 4.

2 EXPERIMENTAL AND ANALYTICAL PROCEDURES

The plate blister test configuration was chosen for this study because it provides a range of mixed-mode conditions.[19,1] Furthermore, crack growth for the glass epoxy bimaterial combination considered here was interfacial and axisymmetric in nature. The latter feature simplified the subsequent finite-element analysis because edge effects did not have to be considered. The specimen geometry is shown in Figure 1a where a modified bisphenol A epoxy, Araldite 502,† that had been mixed with a liquid amido–amine hardener, Araldite 955,† was cast directly to the glass. Initial debonds between the glass and Araldite were formed by a circular piece of Teflon tape that was stuck to a flattened screw head which formed the base of a punch. Driving the punch through applied displacements, Δ, produced circular debonds having a diameter, $2a$. The punch base was designed so that plastic deformations in the contact region were avoided. The thickness, h, of the Araldite

† Products of CIBA-Geigy, Inc.

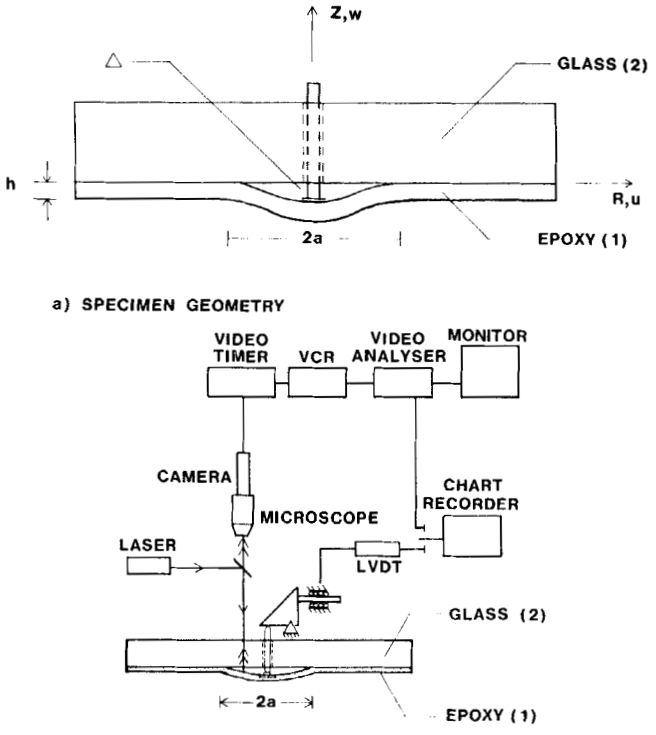

FIGURE 1 Specimen geometry and apparatus.

varied from specimen to specimen but in all cases was uniform to within 0.127 mm. The details of the specimen fabrication and the compact blister loader are given in Ref. 20.

The stress–strain behavior of the epoxy was determined from uniaxial tension tests that were conducted on coupons that were obtained from the delaminated blister specimens. Elastic properties were determined from strain gage measurements of axial and transverse strain. The plastic response of the material was determined using an extensometer. The data were fit (Figure 2) to the Ramberg–Osgood relation.

$$\varepsilon = \frac{\sigma}{E}\left[1 + \frac{3}{7}\left(\frac{\sigma}{\sigma_0}\right)^{n-1}\right] \tag{1}$$

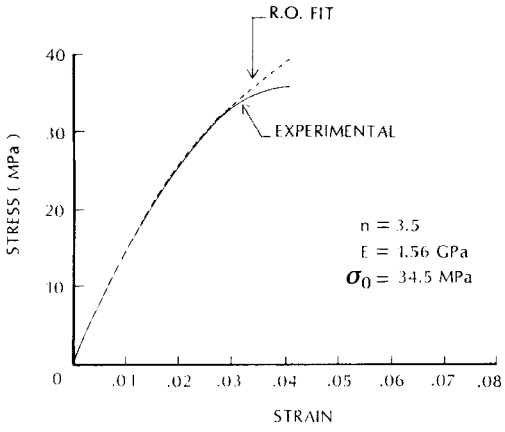

FIGURE 2 Stress strain behavior of Araldite 502.

where E is the Young's modulus of the material, σ_0 is the yield stress, and n is the hardening exponent.

For the values of the parameters noted in Table I, it can be seen that Eq. (1) fits the data well up to 3% strain, after which the material behaves in an essentially perfectly plastic manner. The manufacturer's values for the elastic properties of the glass and the punch base, which was actually embedded in the Araldite, are also listed in Table I.

TABLE I
Material properties

Material	Young's modulus E (GPa)	Poisson's ratio ν	Yield stress σ_0 (MPa)	Hardening exponent n
Araldite	1.56	0.36	3.45	3.5
Glass	68.95	0.20	—	—
Steel	206.85	0.30	—	—

Measurement of normal crack opening displacements

The normal crack opening displacements (NCOD) were measured using crack opening interferometry.[9,10] A schematic of the apparatus that was used for this study is shown in Figure 1b. The coherent light of the laser is reflected by the crack faces to produce two beams which interfere with one another, giving rise to light and

dark interference fringes. The fringes are loci of constant NCOD, Δw, and are resolved by a microscope focussed on the crack plane. The changing fringe patterns, as the specimen is loaded, are recorded through a video system which consists of a camera, timer, cassette recorder, analyzer and monitor. The components are used to determine the NCOD at various applied displacement levels up to and including the instant of crack initiation. For the particular arrangement used here,[20] the NCOD are given by

$$\Delta w = m\lambda/2 \quad m = 0, 1, 2, \ldots \tag{2}$$

where m is the order of the dark fringes and λ is the wavelength of the illuminating beam.

An Argon Ion laser, having a wavelength $\lambda = 0.5145\,\mu$m, was used and thus provided a resolution of $0.2573\,\mu$m in NCOD. In regions of higher displacement gradients, resolution was easily increased to $0.1287\,\mu$m by considering bright fringes in addition to the dark ones. The fact that fringes were formed at all indicates that cracks were coplanar to at least the same ($0.1287\,\mu$m) degree. The fringes could be located to within $5\,\mu$m over a $500\,\mu$m field of view, a somewhat closer view of the crack front region than is provided by a number of other techniques.

The measurements of NCOD up to and including initiation were made over a range of fracture mode mixtures by conducting a series of experiments at various crack diameters. The displacement-controlled tests provided stable crack growth so that cracks, once initiated, could be arrested, thus allowing several experiments to be conducted on the same specimen. Very circular debonds were produced and radial profiles of NCOD at various levels of applied displacement are shown in Figure 3 for an intermediate crack diameter. A reliable indication of crack initiation was provided by comparing a number of profiles around an approximate initiation time. The values of NCOD and applied displacements at initiation are denoted by Δw_c and Δ_c, respectively, and it can be seen that there is some crack blunting associated with initiation. In all experiments there was initially some non-zero value of NCOD due to residual stresses and a small preload which was applied to ensure that, at all times, the crack was fully open right up to its front.[20] These were lumped into an equivalent residual applied displacement, Δ_R, whose determination is now described.

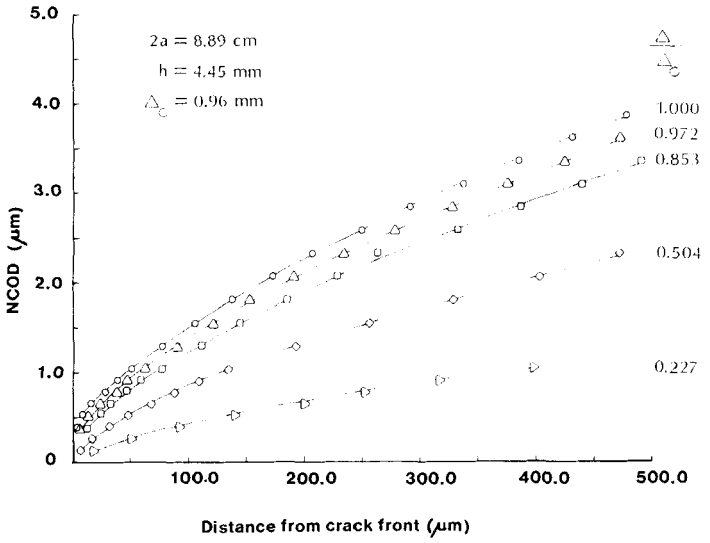

FIGURE 3 Radial profiles of NCOD at various levels of applied displacement.

The dependence of the NCOD on the applied displacements at various distances from the crack front can be examined by cross-plotting the data of Figure 3. The response determined in this way is shown in Figure 4 at 250, 150 and 25 μm from the crack front. As was indicated above, there was an initial crack opening for zero measured applied displacement. For relatively low levels of the applied displacement, the response is linear at all locations and can be extrapolated back to zero NCOD. Although the linear portions of the responses were chosen to pass through the same point at zero NCOD as they should, it can be seen that this was accomplished without unduly compromising the rest of the data. More weight was given to the response at 250 μm in selecting the point of intersection of the responses which was then considered to be the true zero state. A second abscissa originating from this point was then drawn to reflect the total applied displacements. All values of applied displacements quoted in the paper are referred to this measure. Thus, for example, the residual and critical values of applied displacement were, respectively, $\Delta_R = 0.25$ mm and $\Delta_c = 0.96$ mm. It can be seen that, as the applied displacements approach Δ_c, the

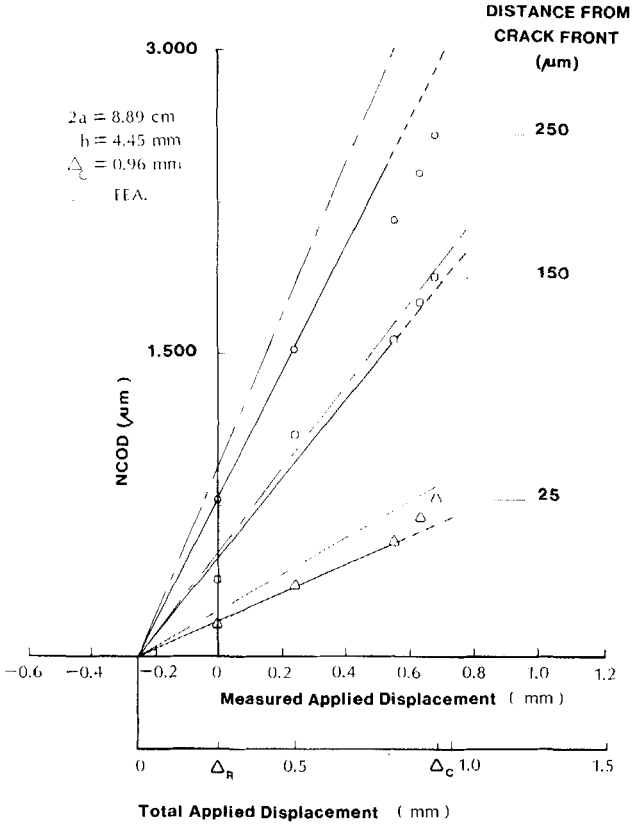

FIGURE 4 NCOD response at various locations from the crack front.

response departs from linearity with the extent of departure increasing with decreasing distance from the crack front.

Finite element analyses

Although it is clear from the results depicted in Figure 4 that non-linear effects are occurring close to the crack front, the analyses here were based, as a first step, on a linear material response using the finite-element code VISTA.[18] Regions removed from the crack front were modelled using eight-node isoparametric quadratic quadrilaterals, while the crack front itself was surrounded (Figure 5)

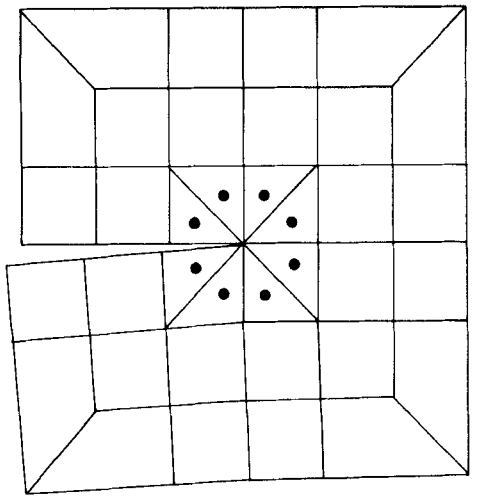

(a) CRACK TIP MESH

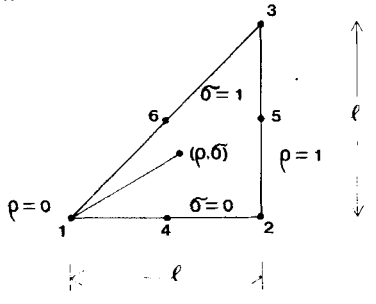

(b) SINGULAR ELEMENT

FIGURE 5 Finite-element mesh close to the crack front.

by eight triangular elements of the variable singularity type.[21] The element is conformable with isoparametric quadrilateral elements and also contains constant strain fields making it complete with respect to globally linear displacement fields. In the present study, the square-root singularity associated with cracks was selected so that the element captured the square root and linear terms in the expansions for displacements near the crack front. The degree of mesh refinement in the crack front region should, therefore, be chosen to reflect these effects and was thus the first consideration.

Mesh refinement studies were made for the 8.89 cm crack diameter considered in Figures 3 and 4. Axisymmetric analyses were conducted using the elastic properties listed in Table 1 for the Araldite layer, the glass substrate and the steel punch base. The total applied displacements, as derived from Figure 4, were considered to act uniformly over the steel punch. As can be seen from Figure 5, the off-hypoteneuse sides of the singular elements were of the same length, l. The singular elements were surrounded by three rings of square quadrilateral elements with side lengths that were also equal to l. The element size outside this region was gradually increased. Four levels of mesh refinement were considered in which the side length, l, was a quarter, an eighth, a sixteenth and a thirty-second of the Araldite layer thickness, h. In some cases l was greater than the 500 μm field of view, and the NCOD, Δw, were derived from the shape functions, N_i, of the singular element and nodal point displacements, w_i, through the equation

$$\Delta w = \sum_{i=1}^{6} N_i[w_i^{(2)} - w_i^{(1)}] \tag{3}$$

where the superscripts 1 and 2 refer to the Araldite and the glass, respectively. The shape functions are given in the Appendix and reflect a change in nodal numbering from the original.[21]

The NCOD near the crack front for the different levels of mesh refinement are compared with the measured values in Figure 6. The applied displacements that were required to produce these displacements were $\Delta = 0.227\Delta_c$, which were well within the region of linear response defined by Figure 4. It can be seen that, at larger distances from the crack front, the coarsest mesh gave rise to the largest crack opening displacements. The NCOD predicted by the two finest levels of mesh refinement were exactly the same, indicating that convergence was obtained for the mesh refinement level of at least $h/l = 16$. The measured NCOD are less than all solutions for distances from the crack front less than 100 μm and agree most closely with the mesh refinement level of $h/l = 8$ thereafter. A cross plot of the comparisons is shown in Figure 7 where the NCOD at 25, 100 and 250 μm are plotted against the applied displacements. The differences are small, but it is interesting to note that at 250 μm from the crack front the largest NCOD are predicted by the coarest mesh, whereas the situation is reversed

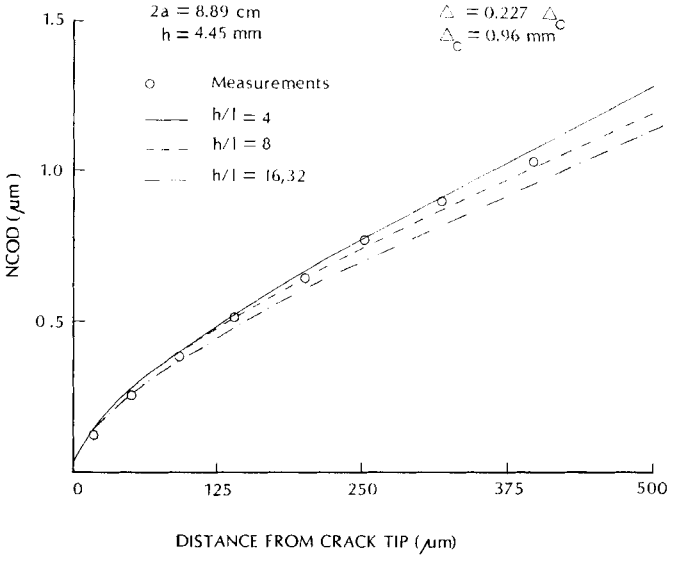

FIGURE 6 Effect of mesh refinement on predicted NCOD.

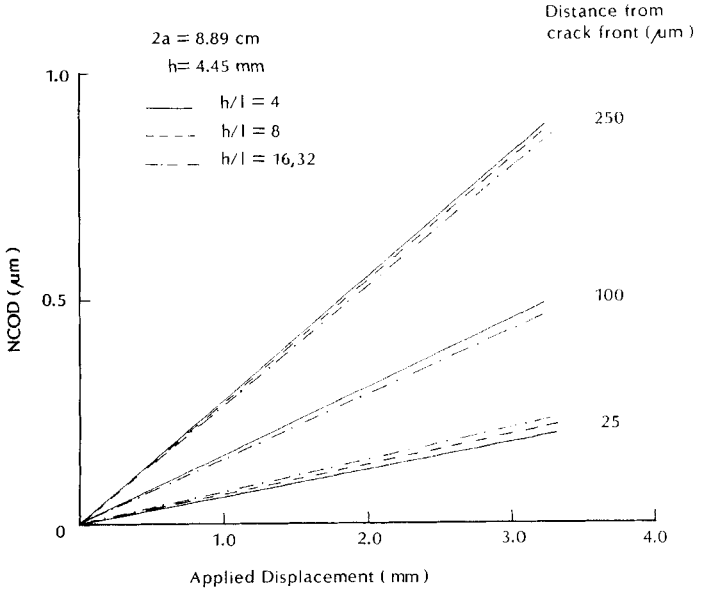

FIGURE 7 Effect of mesh refinement on compliance near the crack front.

at 25 μm. The mesh refinement level in subsequent analyses was taken to be $h/l = 8$.

3 COMPARISON OF RESULTS

Crack initiation experiments were conducted over a range of crack diameters. For short cracks, there was little evidence of crack blunting at the instant of crack propagation. However, the extent of crack blunting did increase with increasing crack diameter and occurred at applied displacement levels that were lower than the critical value. In the region of blunting, double logarithmic plots of NCOD *vs.* distance from crack front[20] indicated a power law dependence with exponents that decreased from 0.5 as the crack diameter was increased. On the basis of elastic analyses, the increase in crack diameter is associated with a relative increase in mode II component. The following comparisons between measurements and finite-element solutions for NCOD were made for representative cases of short, intermediate and long crack diameters. The intermediate case is considered first since it has formed the basis of considerations so far.

A series of NCOD profiles are shown in Figure 8 for applied displacements ranging from the initial value up to the critical value. It can be seen that there is excellent agreement between measurements and predictions for applied displacements up to $0.5\Delta_c$. At higher applied displacements, the finite-element solutions predict larger values of NCOD far away from the crack front. However, very close to the crack front there is some evidence of crack blunting in the measured NCOD, making them larger than the finite-element predictions. When the results are compared in the cross plot (Figure 4) depicting NCOD as a function of applied displacements for various distances from the crack front, the slope of the fitted linear portion of the measured response is always less than the finite-element predictions. The cause of this difference could be due to errors in the measurement of crack diameter, NCOD and applied displacement, uncertainties in the modulus of the Araldite and assignment of Δ_R and, finally, the choice of mesh refinement level. Crack diameters were measured to within 25 μm and, during load application, changes of crack front location up to

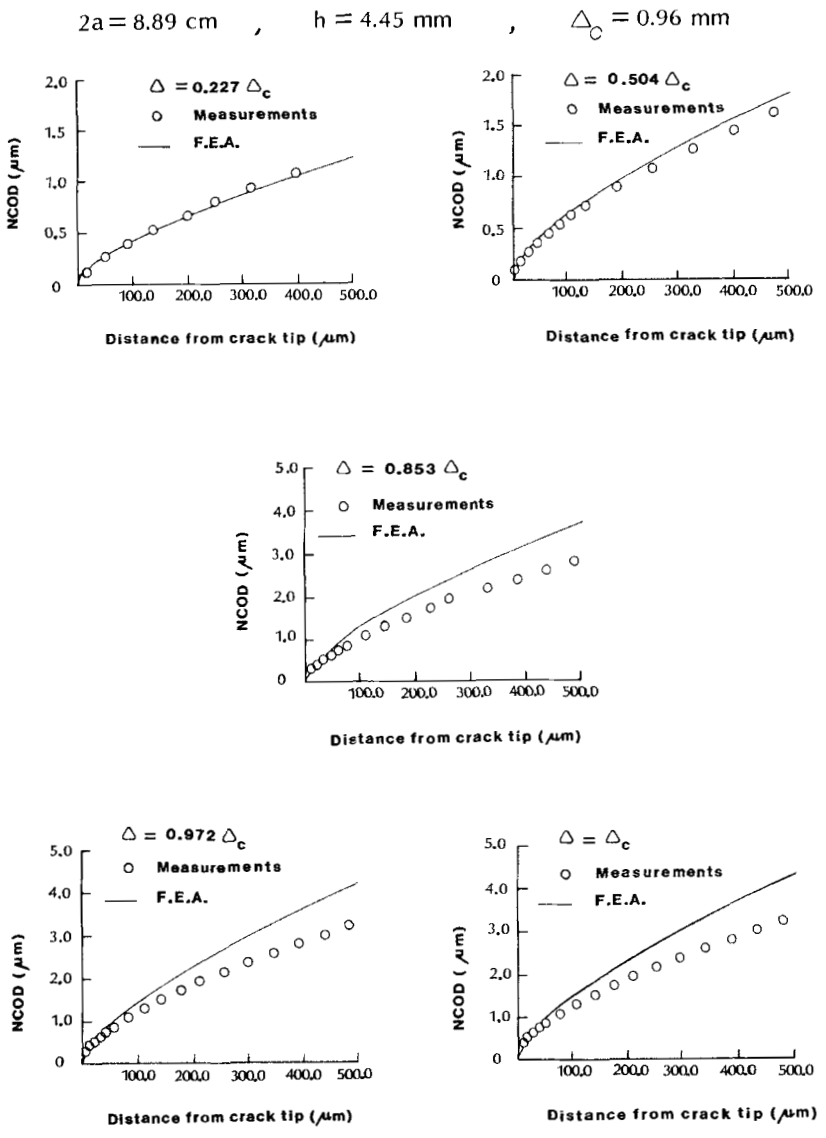

FIGURE 8 Comparison of measured and predicted values of NCOD for an intermediate crack diameter.

15 μm were sometimes observed. However, such variations did not change the predicted NCOD when accounted for in a check case. Uncertainties in NCOD are introduced in locating the fringes rather than through Eq. (2). However, the maximum possible error in fringe location is 1% which would not give rise to the noted differences. The measured value of the Araldite tensile modulus was 1.560 GPa. Some differences could arise from specimen to specimen. In order to obtain bounds on the effect of modulus, Araldite moduli of 0.693 and 6.93 GPa were considered. The effect on the response in the crack front region is shown in Figure 9 where it can be seen that the larger modulus gave rise to a larger slope. The factor of 10 difference in Araldite modulus produces similar differences in slope as were observed in Figure 4. However, it is unlikely that such variations in modulus would occur in practice.

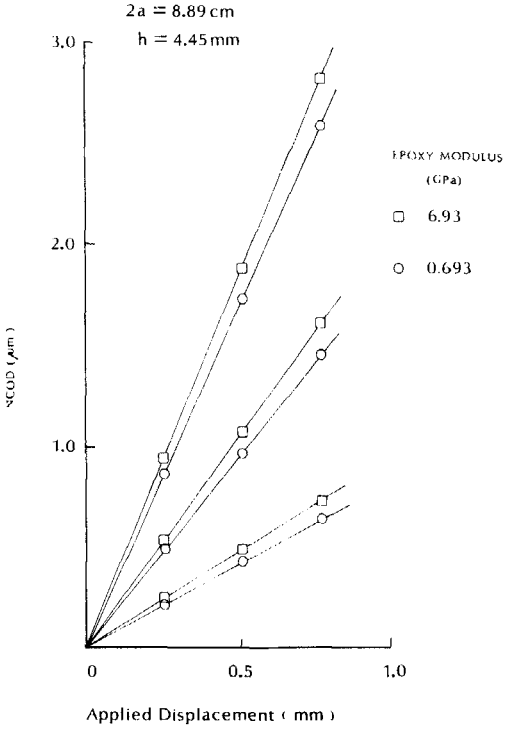

FIGURE 9 Effect of Araldite modulus on NCOD response.

The results of the mesh refinement study (Figure 7) indicate that the measurements and finite-element analyses would have been in slightly closer agreement had a mesh refinement level of $h/l = 16$ been used. The assignment of Δ_R in attempting to obtain the best linear fit to the measurements clearly affects the slopes of these lines. However, an assessment of the error in Δ_R is difficult to make because it was determined from a crossplot and therefore subject to a degree of arbitrariness. An attempt to remove arbitrariness was made by fitting lines having the slope given by the finite-element analysis to the measured values. Such a procedure did not give rise to a consistent value of Δ_R at the three locations from the crack front at which evaluations were made. However, the agreement between predicted and measured NCOD for $\Delta = \Delta_R$ (Figure 8) indicate that Δ_R was well chosen. The final possibility in accounting for the noted differences in slopes arises from the measurement of applied displacements. The resolution of the applied displacements was 0.1% of full scale which would not produce a notable difference. However, the increasing difference between predicted and measured NCOD with increasing applied displacement (Fig. 8) in regions far removed from the crack front leads us to suspect that the loading device was not sufficiently stiff. The suspicions are strengthened by later comparisons of the results from a short-diameter crack which presents the stiffest specimen to the loading device. A compliant loading device would give rise to measurements of applied displacements that were higher than those that were actually applied to the Araldite layer. Thus, since the predicted values of NCOD were obtained from the finite-element analyses based on the measured applied displacements, predicted NCOD would be higher than the measured NCOD. Thus, of the potential reasons for difference noted above, loading device compliance appears to be the most likely cause.

The slope differences are not the only differences in response that can be observed in Figure 4. There is some curvature to the measured response, indicating the presence of nonlinear effects. In this case, the departure from linearity starts at $0.85\Delta_c$ and is most apparent closer to the crack front. Nonetheless, when all effects are combined the comparisons in Figures 4 and 8 indicate a rather good (fortuitous) agreement between measured and predicted values of the critical NCOD up to 150 μm from the crack front.

Similar comparisons are made in Figures 10 and 11 for a short-diameter crack. NCOD profiles at various load levels are compared in Figure 10, where it can be seen that there is quite close agreement up to $0.62\Delta_c$. There is, however, a large difference between measurements and predictions of the critical NCOD. The reason for this difference can be seen more clearly when the results are cross-plotted in Figure 11. The departure of the measured NCOD from their linear fit initially follows the same pattern as before with an increase in slope. However, at initiation there is a

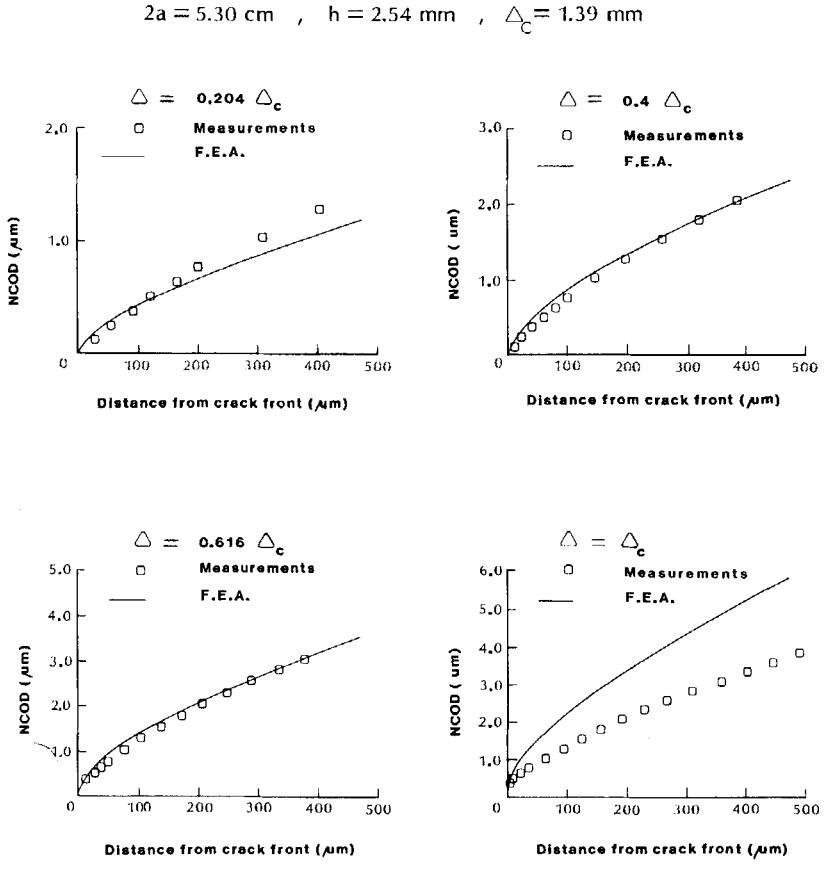

FIGURE 10 Comparison of measured and predicted NCOD profiles for a short crack diameter.

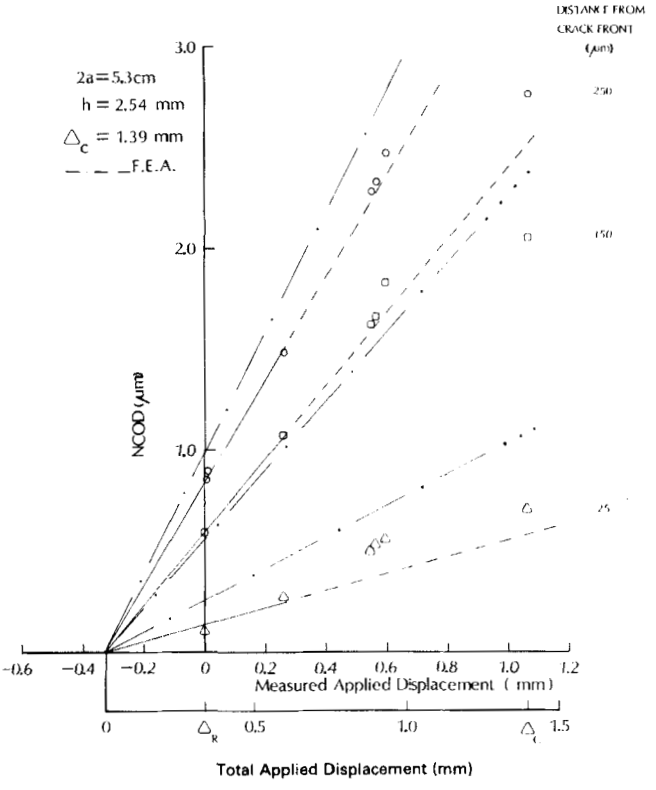

FIGURE 11 Comparisons of NCOD response for a short crack diameter.

large jump in applied displacement for a relatively small change in NCOD, so that the slope decreases. Since the shortest crack presents the stiffest specimen to the loading device, it is suspected that the large apparent applied displacement is due to insufficient stiffness in the loading device. The initial nonlinearity in the crack tip response was due to some highly localized crack blunting.

The scale of crack blunting was much larger for the large-diameter cracks as can be seen from the examples of NCOD profiles shown in Figure 12. In this case, for distances greater than about 35 μm from the crack front, the finite-element solutions for the NCOD were consistently higher than the measured values for all load cases. The foregoing was also true closer to the crack front

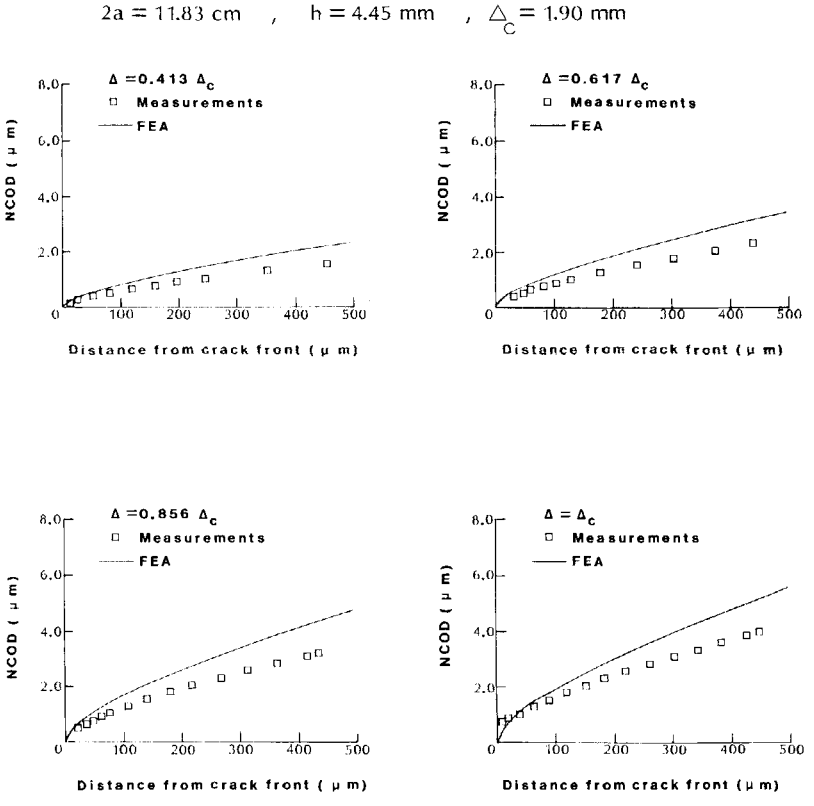

FIGURE 12 Comparison of measured and predicted NCOD profiles for a large crack diameter.

except at the critical load where the blunting at the crack front reversed the situation. In the cross plot of the data (Figure 13), the slopes of the predicted responses are higher than those of the linear fits to the measurements except at 25 μm from the crack front. The increased level of crack blunting is manifest in a higher degree of nonlinearity than was evident in the other two crack-diameter cases that were considered.

In all three cases, it can be concluded that, at load levels approaching the critical values, the finite-element solutions for the NCOD are higher than the measured values except in regions of crack blunting. The main reasons for this behavior are loading-

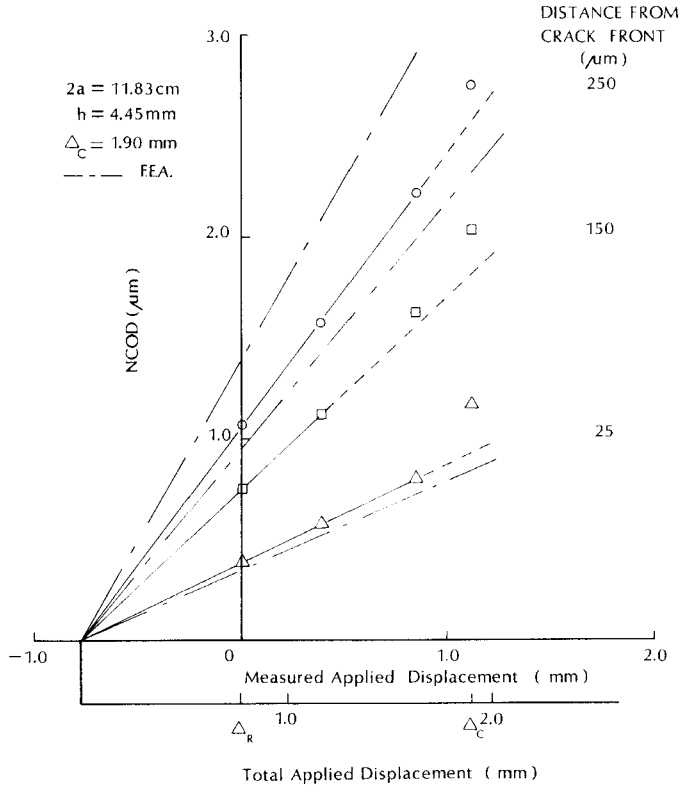

FIGURE 13 Comparisons of NCOD response for a large crack diameter.

device compliance and non-linear effects in the material behavior in the crack front region. In the first case, excessive loading-device compliance leads to measurements of applied displacement that are higher than those that are actually applied to the Araldite layer. Since these overestimates of actual applied displacement are then used as the boundary conditions in the finite-element analyses, the finite-element solutions for NCOD will be correspondingly higher than the measured NCOD. In the case of material non-linear behavior, a plastic zone is produced in the crack front region. In the simplest way of accounting for this, an effective crack is considered whose diameter is made up of the actual crack diameter plus the plastic zone length. The larger crack diameter results in a more

compliant layer which leads to measured NCOD and slopes that are larger than those obtained on the basis of linear analyses.

However, the higher loads are of most interest, particularly for examining mixed-mode fracture parameters and criteria for crack initiation. While the confidence in the measured NCOD is high, they do not, by themselves, provide enough information to determine mixed-mode fracture parameters. On the other hand, although the finite-element solutions provide not only the NCOD but also tangential crack opening displacements (TCOD), stresses and strains for the examination of any fracture parameter, they were based on overestimates of applied displacements and linear material behavior, and were not in agreement with measured NCOD at the critical load. Nonetheless, for purposes of examination of linear elastic fracture mechanics parameters, a hybrid approach is suggested wherein the NCOD from the finite-element solutions are matched with measurements of NCOD outside the plastic region through a simple scaling. The finite-element solutions thus scaled can then be used to examine any mixed-mode fracture parameter of interest.

In order to effect the scaling, the measurements of and finite-element solutions for the critical NCOD were fit to the relation

$$\Delta w_c = Ar^{1/2} + Br \tag{4}$$

through a least-squares procedure where the measurements were taken in the region $r > 25\,\mu$m. The coefficients A and B thus determined are noted in Table II for the three crack diameters considered here. The correlation coefficients for the measured NCOD are also noted and indicate that Eq. (4) is a reasonable representation. The ratios of the coefficients of the square root and

TABLE II
Comparison of coefficients in near tip expansions for critical NCOD

Crack diameter (cm)	Measurement			Finite element		$\frac{A_F}{A_M}$	$\frac{B_F}{B_M}$	Scale factor
	A_M	B_M	r[a]	A_F	B_F			
5.30	1.228 E-1	3.287 E-3	0.96	1.872 E-1	2.836 E-3	2.524	0.863	0.753
8.89	1.294 E-1	2.162 E-3	0.99	1.337 E-1	4.073 E-3	1.118	1.884	0.782
11.89	1.486 E-1	1.707 E-3	0.95	1.503 E-1	4.393 E-3	1.011	2.574	0.799

[a] r is the correlation coefficient.

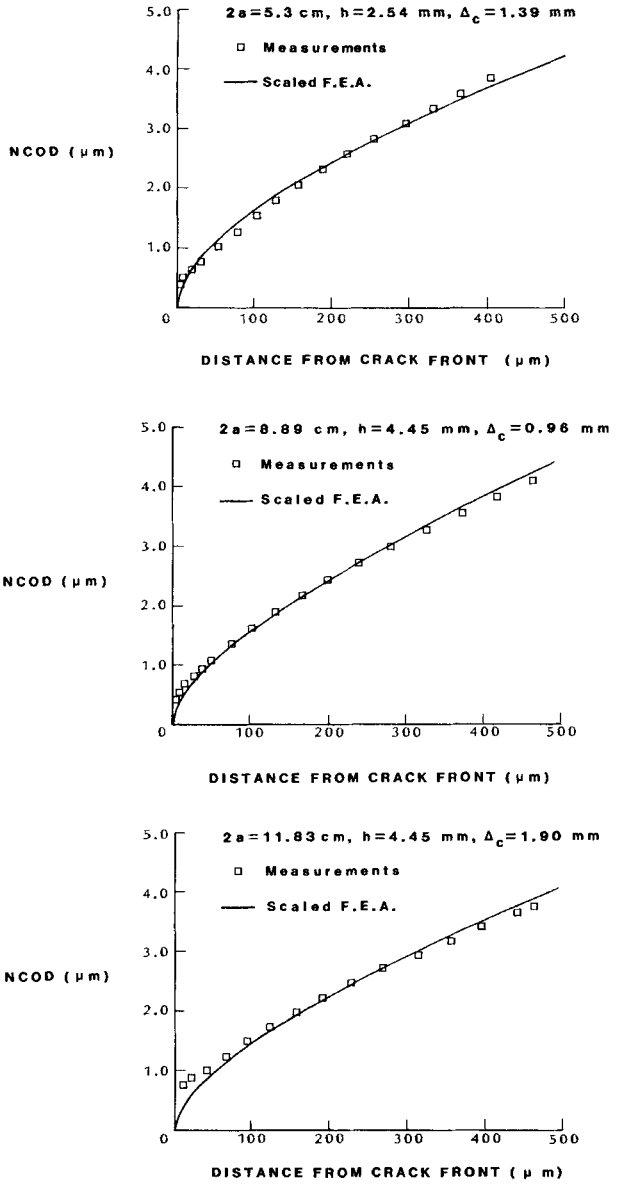

FIGURE 14 Comparison of scaled finite-element solutions and measurements of critical NCOD for three crack diameters.

linear terms based on the finite-element solution and the measurements are also noted in Table II. It can be seen that, as the crack diameter becomes larger, the agreement in the square root coefficient improves while the ratio B_F/B_M also becomes larger. The shapes of the NCOD profiles are therefore different. For distances from the crack front less than 5 μm, the contribution to the NCOD from the linear term in (4) was less than 5% of the square root term in all cases. However, at 500 μm, the contribution from the linear term was as high as 50%. Thus, a simple scaling of the finite-element solution by the ratio A_F/A_M, for example, would not produce a good match with the measured NCOD over the whole field of view. Since the NCOD response was linear for distances from the crack front greater than 250 μm (and linear elastic fracture parameters are often evaluated in this region using other methods), the NCOD were matched at this point. The scale factors that were applied to the finite-element solution in order to match the NCOD are noted in Table II. It can be inferred from the scale factors that the original finite-element solutions were 20–25% higher than the measured critical NCOD at this point. The matched finite-element solutions are compared with the measured critical NCOD in Figure 14 for the three crack diameters considered here. Based on the fit to the measurements, the scaled finite-element solutions are first lower and then higher than the measured NCOD for the intermediate and larger crack diameter. The situation is reversed for the short-diameter crack, but the difference in all cases was less than 8%. The difference between the scaled finite-element solution and the actual displacements in the blunting region is, of course, even greater.

4 CONCLUSIONS

The results of crack initiation experiments for mixed-mode interfacial crack growth that were reported in a previous paper[20] were compared with analyses that were made using the finite-element method. The circular cracks resulting from a point-loaded blister configuration allowed axisymmetric analyses to be conducted. The analyses were based on the measurements of applied displacements that were made during the crack initiation experiments. The stress–strain behavior of the epoxy layer was considered to be

linearly elastic, and singular elements were used around the crack front. The optimum size of the singular element and surrounding eight-node quadrilaterals was found to be one-sixteenth of the epoxy layer thickness.

The basis of comparison between the finite-element solutions and the experiments was the normal crack opening displacements (NCOD) near the crack front which had been measured using optical interferometry. The comparisons were made for three different crack diameters and at various applied displacement levels up to and including crack initiation. Short, intermediate and long crack diameters were chosen because increasing amounts of crack blunting had been associated with them during the experiments. The closest agreement between finite-element solutions and measurements was obtained at the lower levels of applied displacements. Various potential causes of the differences noted at higher load levels were considered. The most likely causes were found to be loading-device compliance and nonlinear material behavior in the crack front region. The feasibility of a matching procedure was explored that would allow the finite-element solutions to be used to examine mixed-mode fracture parameters and criteria.

Acknowledgements

This work was supported by the Solid Mechanics Division of the National Science Foundation (Grant MEA-8402064) and the Department of Aerospace Engineering and Engineering Mechanics, The University of Texas at Austin; the support is gratefully acknowledged. The accurate and timely typing of the manuscript by Lynn McKay is also greatly appreciated.

References

1. G. P. Anderson, K. L. DeVries and M. L. Williams, *Int. J. of Fracture* **10,** 565–583 (1974).
2. D. R. Mulville, D. L. Hunston and P. W. Mast, *J. Eng. Mat. Tech.* **100,** 25–31 (1978).
3. G. P. Anderson, K. L. DeVries and M. L. Williams, *J. Colloid and Int. Sci.* **47,** 600–609 (1974).
4. E. E. Gdoutos and G. Papakaliatakis, *Engineering Fracture Mechanics* **6,** 177–187 (1982).
5. P. S. Theocaris and C. A. Strassinakis, *Engineering Fracture Mechanics* **14,** 363–372 (1981).
6. D. L. Davidson, D. R. Williams and J. E. Buckingham, *Experimental Mechanics* **23,** 242–248 (1983).

7. D. Post, *Experimental Mechanics* **23,** 203–210 (1983).
8. M. E. Fourney, in *Speckle Metrology*, R. K. Erf, Ed. (Academic Press, New York, 1978).
9. E. Sommer, *Eng. Frac. Mech.* **1,** 705–718 (1970).
10. K. M. Liechti and W. G. Knauss, *Experimental Mechanics* **22,** 262–269 (1982).
11. A. Piva and E. Viola, *Engineering Fracture Mechanics* **13,** 143–174 (1980).
12. J. K. Knowles and E. Sternberg, *Int. J. Solids and Structures* **11,** 1173 (1975).
13. S. G. Sawyer and R. B. Anderson, *Eng. Fract. Mech.* **4,** 605–616 (1972).
14. K. Y. Lin and J. W. Mar, *Int. J. Fracture* **12,** 521–531 (1976).
15. C. C. Hong and M. Stern, *J. Elasticity* **8,** 21–34 (1978).
16. R. E. Smelser, *Int. J. Fracture* **15,** 135–143 (1979).
17. J. F. Yau and S. S. Wang, *Eng. Fracture Mechanics* **20,** 423–432 (1984).
18. E. B. Becker, *et al.*, "Viscoelastic Stress Analysis Including Moisture Diffusion for Adhesively Bonded Joint", Air Force, Wright Aeronautical Lab. Report #AFWAL-TR-84-4057 (1984).
19. F. Erdogan and K. Arin, *J. Eng. Sci.* **10,** 115–125 (1972).
20. K. M. Liechti and E. C. Hanson, "An Examination of Mixed-Mode Debonding in the Blister Test", to be published in *ASTM STP xxx* (1987), International Symposium on Adhesively Bonded Joints: Testing, Analysis and Design.
21. M. Stern, *Int. J. for Num. Meth. in Eng.* **14,** 409–421 (1979).

Appendix

INTERPOLATING SHAPE FUNCTIONS FOR SINGULAR ELEMENTS

For singularities of strength λ, the shape functions for the singular element are given by the equations below. The nodal numbering is shown in Figure 5.

$$N_1(\rho, \sigma) = 1 + \frac{2 - 2^{1-\lambda}}{2^{1-\lambda} - 1}\rho - \frac{1}{2^{1-\lambda} - 1}\rho^{\lambda}$$

$$N_2(\rho, \sigma) = \frac{2^{1-\lambda}}{2^{1-\lambda} - 1}(1 - \sigma)\rho - \left(\frac{1}{2^{1-\lambda} - 1}2\sigma\right)(1 - \sigma)\rho^{\lambda}$$

$$N_3(\rho, \sigma) = \frac{2^{1-\lambda}}{2^{1-\lambda} - 1}\sigma\rho - \left(\frac{1}{2^{1-\lambda} - 1} + (1 - \sigma)\right)\sigma\rho^{\lambda}$$

$$N_4(\rho, \sigma) = \frac{-2}{2^{1-\lambda} - 1}(1 - \sigma)\rho + \frac{2}{2^{1-\lambda} - 1}(1 - \sigma)\rho^{\lambda}$$

$$N_5(\rho, \sigma) = 4\sigma(1 - \sigma)\rho^{\lambda}$$

$$N_6(\rho, \sigma) = \frac{-2}{2^{1-\lambda} - 1}\sigma\rho + \frac{2}{2^{1-\lambda} - 1}\sigma\rho^{\lambda}$$